

Structural and magnetic characterization of Co^{2+} substituted nano structured Copper-Zinc spinel ferrite

Sindhu S¹, D. D. Birajdar²

¹ GND Engineering College, Bidar, Karnataka State, India

² B.S.S. Arts, Science and Commerce college Makani, Osmanabad (M.S.), India

Abstract : Nano particles of $\text{Cu}_{0.61-x}\text{Co}_x\text{Zn}_{0.39}\text{Fe}_2\text{O}_4$ ($0 \leq x \leq 0.5$) synthesized through sol-gel auto combustion method. Nitrates of elements and citric acid are used as starting materials. X-ray Diffraction, Thermo Gravimetric Analysis and Vibrating Sample Magnetometer are used to analyze the properties. Effect of variation in the Co substitution and its impact on particle size, lattice constant, density, cation distribution, ferritization temperature, associated water content, magnetic properties like saturation magnetization (M_s), coercivity (H_C) and remanent magnetization (M_r) is observed. Lattice parameter increases with increasing Co^{+2} concentration whereas X-ray density, bulk density decreases with the Co^{+2} content. In Cation distribution the Co and Cu ion show preference towards octahedral B-site, Zn occupy A site whereas Fe occupy both A and B site. Cation redistribution takes place for $x > 0.3$. Saturation magnetization increases from ($x \leq 0.3$). For $x > 0.3$, M_s decreases suggesting that significant canting exists at B site. However, coercivity, magnetocrystalline anisotropy and remanent magnetization increases with the Co^{2+} substitution.

Keywords: Coercivity (H_C), Remanent and Saturation Magnetization, Sol-gel synthesis, Thermo Gravimetric Analysis and Vibrating Sample Magnetometer, X-ray Diffraction.

I. Introduction

Co^{2+} substituted $\text{Cu}_{0.61-x}\text{Co}_x\text{Zn}_{0.39}\text{Fe}_2\text{O}_4$ ferrites are commercially important magnetic materials and play an important role in the production of magnetic recording media. The cation distribution in CuFe_2O_4 copper ferrite can be represented by formula $(\text{Cu}^{2+}_x + \text{Fe}^{3+}_{1-x})^A [\text{Cu}^{2+}_{1-x} + \text{Fe}^{3+}_{1+x}]^B \text{O}_4$. The parameter of inversion is ($0 \leq x \leq 0.5$). When the spinel is synthesized using classical ceramic technologies (high temperature treatment of the initial oxides of the metal cations) with strict stoichiometry ($x = 1$), it has tetragonal structure with crystal parameters $a = 8.20$ and $c = 8.60$; $c/a = 1.05$ [1]. The c/a ratio can be changed via decreasing the copper concentration, or alternatively, by temperature treatments. Yokoyama et al. [2] observed changes in the crystal structure of nanosized CuFe_2O_4 powders obtained by co-precipitation and subsequent annealing. According to some other authors [3] $a = 8.24$, $c = 8.68$, but c/a is again 1.05. The structure of CuFe_2O_4 is considered as that of a tetragonally deformed spinel stretched along the (0 1 1) direction. They proved that the copper spinel is cubic at temperatures below 300°C and tetrahedral over 400°C . Further Co ferrite shows good magnetostrictive properties, magnetocrystalline anisotropy, high coercivity and moderate saturation magnetization among all the ferrite family [10]. Therefore, by keeping this composition in our mind, we have proposed the studies on structural analysis, cation distribution and magnetic properties of nano-size $\text{Cu}_{0.61-x}\text{Co}_x\text{Zn}_{0.39}\text{Fe}_2\text{O}_4$ ($0 \leq x \leq 0.5$) by sol-gel method.

II. Experimental:

2.1 Preparation method:

Sol-gel auto-combustion method is a novel method of preparing nano-materials [11] by which nanocrystalline powder of $\text{Cu}_{0.61-x}\text{Co}_x\text{Zn}_{0.39}\text{Fe}_2\text{O}_4$ ($0 \leq x \leq 0.5$) is prepared. It can save energy and avoid agglomeration during the calcinations at high temperature. A.R. grade citric acid ($\text{C}_6\text{H}_8\text{O}_7$)· H_2O , copper nitrate ($\text{Cu}(\text{NO}_3)_2 \cdot 3\text{H}_2\text{O}$), zinc nitrate ($\text{Zn}(\text{NO}_3)_2 \cdot 6\text{H}_2\text{O}$), cobalt nitrate ($\text{Co}(\text{NO}_3)_2 \cdot 3\text{H}_2\text{O}$) and ferric nitrate ($\text{Fe}(\text{NO}_3)_3 \cdot 9\text{H}_2\text{O}$) were used as starting materials. The metal nitrates were dissolved in a minimum amount of double distilled water to get a clear solution and ammonia solution was slowly added to maintain the pH. The mixed solution was kept on to a hot plate with continuous stirring. The solution became viscous and finally formed a very viscous brown gel. When finally all water molecules were removed from the mixture, the viscous gel began frothing. After few minutes, the gel automatically ignited and burnt with glowing flints. The auto-combustion was completed within a minute, yielding the brown-colored ashes termed as a precursor. The powder which is thus prepared, then annealed at 600°C for 4 hours.

2.2 Structural and magnetic characterization:

The dried gels were characterized by Thermo gravimetric analysis and differential thermal analysis at a heating rate of $10^\circ\text{C}/\text{min}$ in air atmosphere. The samples were powdered for X-ray investigations. Magnetic

measurements were performed using the commercial PARC EG&G vibrating sample magnetometer VSM 4500. Hysteresis curve loops were measured at room temperature with maximum applied magnetic fields. Magnetic field sweep rate was 5 Oe/s for all measurements. Hence measurement of hysteresis loops with maximum field of 0.7 T took about 2 hours. The samples prepared in powder form were fixed in paraffin in order to exclude the motion of powder in a measuring cap.

III. Results and discussion:

3.1 Structural properties:

The experimental observation showed that the nitrate–citrate gels with all three molar ratios of metal nitrates to citric acid exhibited self-propagating combustion behavior. It was also observed that the combustion rate is associated with the ratio of nitrates of citric acid. The TGA of the mid sample $x = 0.3$ decomposing in air atmosphere in the temperature range 20 to 700°C with a heating rate of 10 °C/min is shown in Fig. 1.

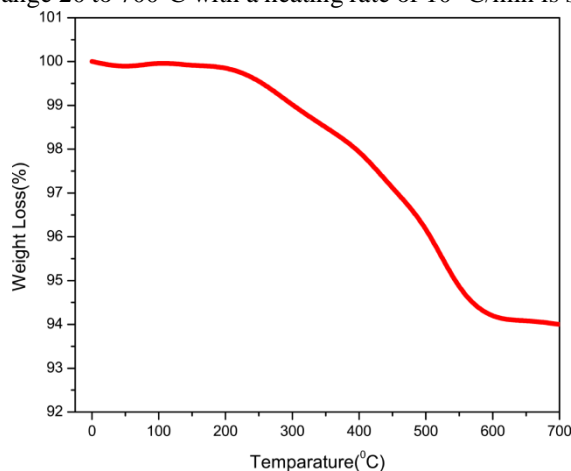


Fig.1 TGA/DTA curve of the typical sample ($x = 0.4$).

The observed weight loss below 100°C of $x = 0.3$ sample for Co is attributed to the loss of physically or chemically absorbed OH groups. The weight loss around 350 °C, which is ascribed to the vaporization of absorbed water. The third weight loss around 350 to 600 °C, which is associated with the residual organic matter including citric acid. The weight loss below 600 °C is due to the loss of absorbed water and the decomposition of organic derivatives. Final weight loss above 600 °C, due to weight loss of as received powder. The end-products after decomposition were identified as single spinel phase Cu–Co–Zn ferrite. From the analysis of their recorded XRD patterns (Fig. 2).

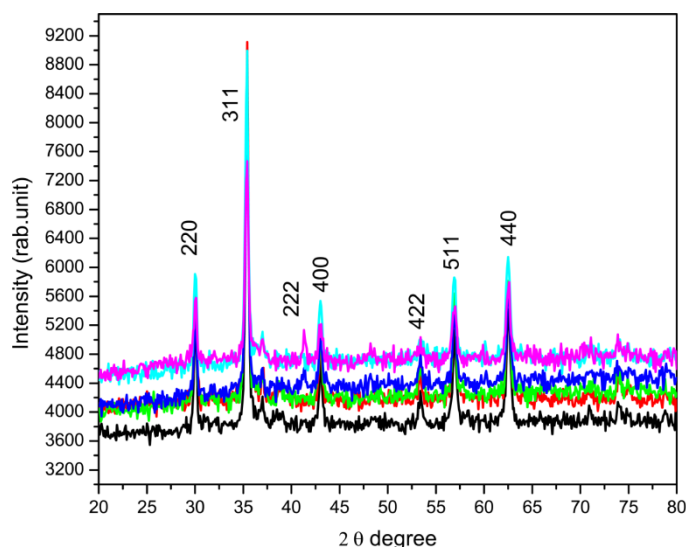


Fig.2 X-ray powder diffraction for $Cu_{0.61-x}Co_xZn_{0.39}$ (a) $x = 0.0$, (b) $x = 0.1$, (c) $x = 0.2$, (d) $x = 0.3$, (e) $x = 0.4$ and (f) $x = 0.5$.

This proves the simultaneous completion of decomposition process of oxalate complex and ferritization. The XRD patterns exhibit peaks corresponding to typical Cu–Co–Zn ferrites and the absence of any other impurity phase. Substitution of Cu by Co increases the overall crystallinity of the spinel phase and all the peaks are

indexed as reported on ASTM cards (cards 1-1121 and 3-0864). The variation of lattice constant with composition x is shown in Fig. 3.

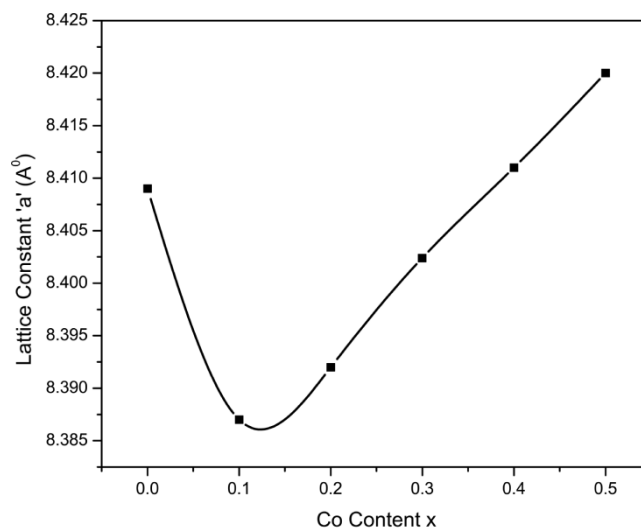


Fig.3 Variation of lattice constant 'a' with Co content x.

It is clear from Fig. 3 that lattice constant decreases with increase in x for $x = 0.1$. For $x > 0.1$ lattice constant increases with composition x . Generally in a solid solution series, linear increase or decrease of lattice constant within the miscibility range with composition is observed [12]. This may result into initial decrease in lattice constant up to $x = 0.1$ beyond which it increases. This nonlinear behavior of lattice constant suggests that the ferrite system is not completely normal or inverse. In the present series, $\text{Cu}_{0.61-x}\text{Co}_x\text{Zn}_{0.39}\text{Fe}_2\text{O}_4$ ($0 \leq x \leq 0.5$) smaller Cu^{2+} (0.72\AA) ions are replaced by larger Co^{2+} (0.745\AA) [13]. Doping Co^{2+} ions in a spinel type structure will induce uniform strain in the lattice as the material is elastically deformed. This effect causes the lattice plane spacing to change and the diffraction peaks shift to a lower 2θ position. Since each primitive unit cell of the spinel structure contains eight molecules, the X-ray density, d_x was determined according to the following

relation [14] $d_x(\text{Ferrite}) = \frac{8M}{N \times a^3}$ where M is molecular weight of the particular ferrite, N is the

Avogadro's number and a^3 is the volume of the cubic unit cell and are shown in Fig.4.

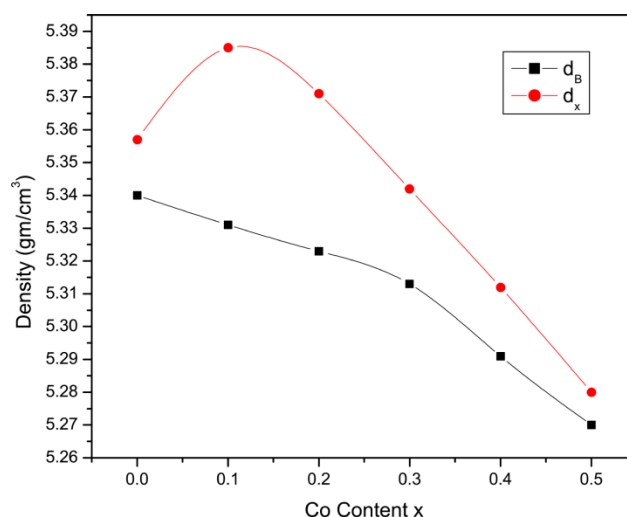


Fig.4 Variation of X-ray density 'dx' and bulk density 'dB' with Co content x.

From Fig. 4, it is observed that X-ray density ' d_x ' decreases with addition of Co^{2+} ion content, which may be attributed to the ionic radii of constituent ions causing decrease in lattice parameter and the molecular weight of cobalt ferrite (234.625) is lower than copper ferrite (239.23). The bulk density ' d_B ' of the specimens has been determined by the hydro-static method. The values of the bulk density are shown in Fig. 4. The bulk density was found to decrease with Co content x . These measurements show densities decreases with Co^{2+} substitution which in accordance with the densities of pure Cu and Co ferrites, 8.95gm/cm^3 and 5.29gm/cm^3 , respectively.

The broad peaks are seen in XRD indicates the nano particle size of the ferrite formed due to sol-gel preparation. It is also evident from the crystallite size of 25-34 nm for all samples estimated from the most intense peak (311) using the Scherrer equation, $D_{hkl} = 0.9\lambda/B\cos\theta$, [15] where D_{hkl} , λ , B, and θ are the volume-averaged particle diameter, X-ray wavelength, full width at half maximum (FWHM), and diffraction angle, respectively.

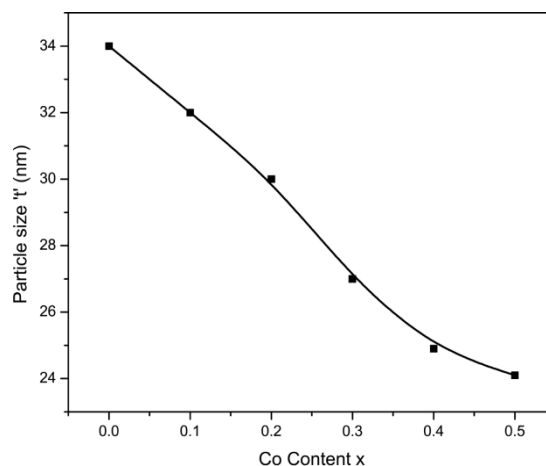


Fig.5 Variation of particle size with Co content x.

The present results in fig.5 depict that the increasing concentration of cobalt Co^{2+} decreases with the particle size. This was probably due to the reaction condition, which favored the formation of new nuclei preventing further growth of particles when the Co concentration was increased. This may be due to migration of small number of Co^{2+} ions in the midst of Co^{3+} ions in B-sites. This observation is similar to that of Caltun et. al. [16] for Co-Mn ferrite. The hopping length for tetrahedral A-site (L_A) and octahedral B-sites (L_B) are calculated using the values of lattice constant. The variation of hopping lengths with Co content x is shown in Fig. 6 & 7.

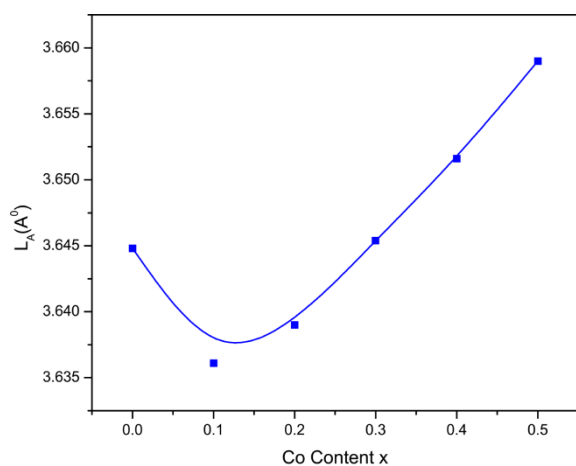


Fig.6 Variation of L_A with Co content x.

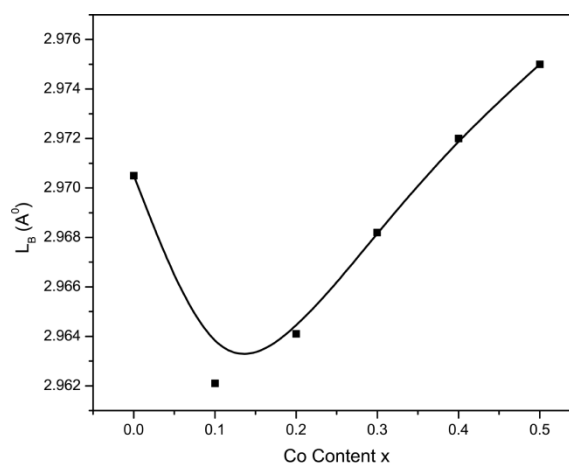


Fig.7 Variation of L_B with Co content x.

It is observed from Fig. 6 & 7 that the distance between the magnetic ions (hopping length) increases as Co content x increases. Using the experimental values of lattice constant 'a' and oxygen positional parameter 'u' and substituting it into equations discussed elsewhere [17]. Tetrahedral and octahedral bond length (d_{Ax} and d_{Bx}), tetrahedral edge, shared and unshared octahedral edge (d_{AXE} , d_{BXE} and d_{BXEU}) were calculated and the values are given in Table 1

Table 1

Tetrahedral bond (d_{AX}), Octahedral bond (d_{BX}), Tetra edge (d_{AXE}) and octaedge (Shared d_{BXE} and unshared d_{BXEU}). The error estimates is ($\pm 0.002 \text{ \AA}$).

X	d_{AX} (\AA)	d_{BX} (\AA)	Tetra edge (\AA)		Octa edge (\AA)	
			d_{AXE}	d_{BXE}	d_{BXEU}	
0	1.907	2.054	3.113	2.831	2.981	
0.1	1.904	2.050	3.106	2.820	2.973	
0.2	1.905	2.051	3.109	2.825	2.974	
0.3	1.907	2.053	3.113	2.828	2.978	
0.4	1.909	2.055	3.116	2.831	2.982	
0.5	1.911	2.057	3.121	2.835	2.985	

It is observed that the allied parameter increases as from its starting value with Co content x increases. This could be related to the larger radius of Co^{2+} ions as compared to Cu^{3+} ions and the site occupancy of the constituent ions in the present ferrite system.

3.2 Cation distribution:

The cation distribution in the present system was obtained from the analysis of X-ray diffraction patterns. In this method the observed intensity ratios were compared with the calculated intensity ratios. In the present study Bertaut method [18] is used to determine the cation distribution. This method selects a few pairs of reflections according to the expression

$$\frac{I_{hkl}^{Obs.}}{I_{h'k'l'}^{Obs.}} \propto \frac{I_{hkl}^{Calc.}}{I_{h'k'l'}^{Calc.}} \quad (1)$$

where, $I_{hkl}^{Obs.}$ and $I_{hkl}^{Calc.}$ are the observed and calculated intensities for reflection (hkl), respectively. If an agreement factor (R) is defined as in Eq. (2), the best-simulated structure which matches the actual structure of the sample will lead to a minimum value of R and the corresponding cation distribution is obtained for each hkl and $h'k'l'$ reflection pair considered.

$$R = \left| \left(\frac{I_{hkl}^{Obs.}}{I_{h'k'l'}^{Obs.}} \right) - \left(\frac{I_{hkl}^{Calc.}}{I_{h'k'l'}^{Calc.}} \right) \right| \quad (2)$$

The intensities of these are nearly independent of the oxygen parameters. To determine the cation distribution and its variation with composition, it is necessary to calculate for each composition the above mentioned intensity ratios expected for given arrangements of the cations and compare them with the experimental values.

$$I_{hkl} = |F|_{hkl}^2 P \cdot L_p \quad (3)$$

where, F is structure factor, P is multiplicity factor, L_p the Lorentz polarization factor and

$$L_p = \frac{1 + \cos^2 2\theta}{\sin^2 \cos 2\theta} \quad (4)$$

The atomic scattering factor for various ions was taken from the literature [19]. The cation distribution for each concentration and the site preferences of cations distributed among tetrahedral A-site and octahedral B-site showing the fraction of Cu^{2+} and Fe^{3+} ions on either sites are listed in Table 2.

Table 2

Cation distribution of $Cu_{0.61-x}Co_xZn_{0.39}Fe_2O_4$

X	Cation distribution	
	A-site	B-site
0.0	$(Zn_{0.39}Fe_{0.61})$	$[Cu_{0.61}Fe_{1.39}] O_4$
0.1	$(Cu_{0.06}Zn_{0.39}Fe_{0.55})$	$[Cu_{0.45}Co_{0.1}Fe_{1.45}] O_4$
0.2	$(Cu_{0.075}Zn_{0.39}Fe_{0.535})$	$[Cu_{0.425}Co_{0.2}Fe_{1.375}] O_4$
0.3	$(Cu_{0.08}Zn_{0.39}Fe_{0.53})$	$[Cu_{0.32}Co_{0.3}Fe_{1.38}] O_4$
0.4	$(Cu_{0.09}Co_{0.05}Zn_{0.25}Fe_{0.61})$	$[Cu_{0.21}Co_{0.35}Zn_{0.05}Fe_{1.39}] O_4$
0.5	$(Cu_{0.1}Co_{0.09}Zn_{0.21}Fe_{0.60})$	$[Cu_{0.1}Co_{0.41}Zn_{0.09}Fe_{1.40}] O_4$

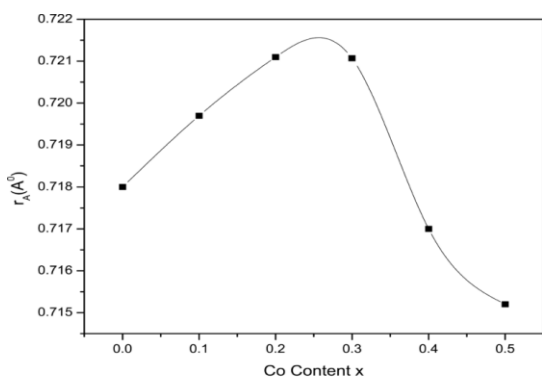


Fig.8 Variation of ionic radii of A site (r_A) with Co content x .

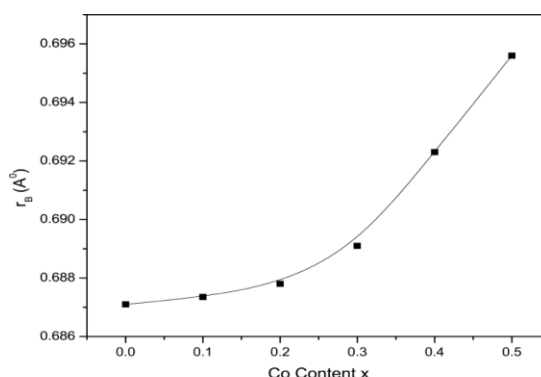


Fig.9 Variation of ionic radii of B-site (r_B) with Co content x .

The variation of mean ionic radius of the A-site (r_A) and of the B-site (r_B) with Co is shown in Fig. 8 & 9. The r_A increases up to $x \leq 0.3$, this is due the increase in migration of larger Cu^{2+} (0.72 Å) ions from B site to A site which replaces smaller Fe^{3+} (0.67 Å) ions at B site.

$$r_A = \left(u - \frac{1}{4}\right)a\sqrt{3} - R_0 \tag{5}$$

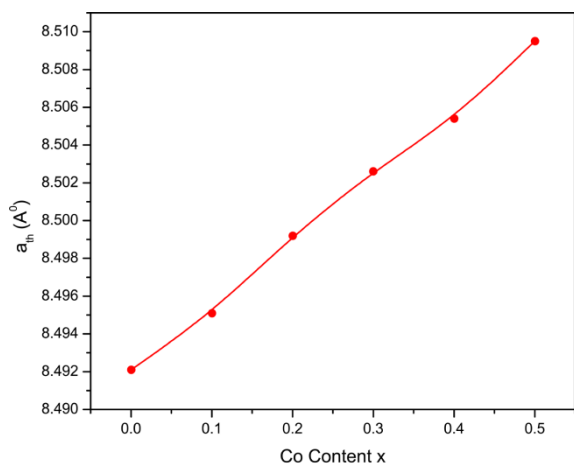


Fig.10 Variation of theoretical lattice constant ' a_{th} ' with Co content x .

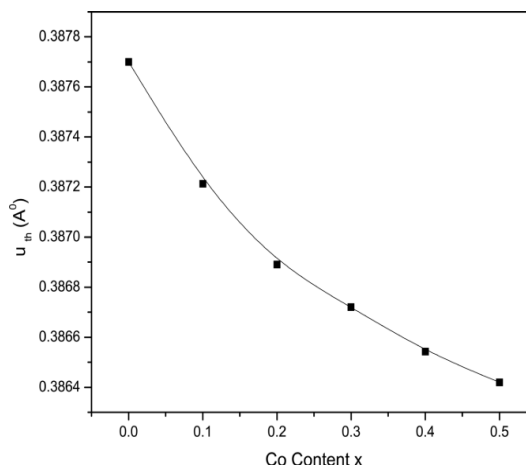


Fig.11 Variation of oxygen positional parameter ' u ' with Co content x .

Fig. 10 shows the increase in the theoretical value of lattice constant a_{th} with Co content & Fig. 11 shows decreasing value of oxygen positional parameter ' u ' from 0.387 to 0.386 (Å). However, in the present work $u > 0.375$ may be due to anion displacement from the ideal situation so that it forms an expanded tetrahedral interstices. The lattice disturbance is confirmed from the data for lattice constant and the oxygen positional parameter u . The theoretical lattice parameter ' a_{th} ' was calculated using the values of tetrahedral and octahedral reading (r_A, r_B) and is given by the following relation,

$$a_{th} = \frac{8}{3\sqrt{3}} \left[(r_A + R_0) + \sqrt{3}(r_B + R_0) \right] \tag{6}$$

where, r_A and r_B are radii of tetrahedral (A) site and octahedral [B] site, R_0 is radius of oxygen i.e. ($R_0 = 1.32$ Å). It is noticed that a_{th} is higher than a at lower concentration of Co^{2+} , and becomes closer at higher Co content. The deviation may be due to the formation of Co^{3+} in tetrahedral sites which has lower radius than Co^{2+} .

3.3 Magnetic properties:

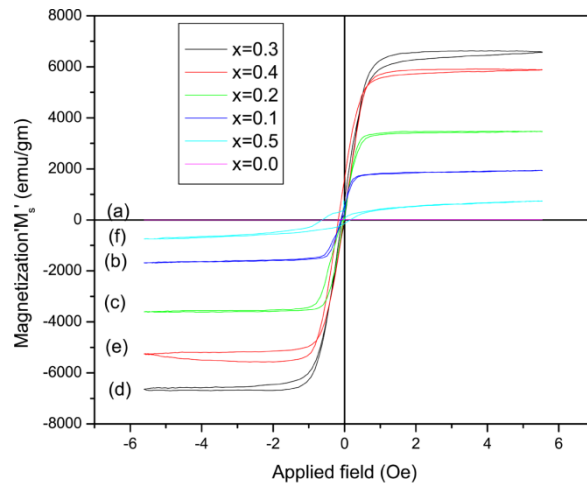


Fig.12 Variation of magnetization with applied field, (a) $x = 0.0$, (b) $x = 0.1$, (c) $x = 0.2$, (d) $x = 0.3$, (e) $x = 0.4$, (f) $x = 0.5$.

Room temperature hysteresis loops with the field of 7 kOe, for all the samples are shown in Fig. 12. Fig. 12 shows the variation of saturation magnetization with Co^{2+} content x . These plots show that an increase in Co^{2+} doping yields monotonic increase in the saturation magnetization of Cu-Co-Zn ferrite (for $x \leq 0.3$), which may be due to the substitution of Cu^{2+} ions by Co^{2+} ions on the octahedral sites. The magnetic moment μ_B per ion for Co^{2+} ions ($3 \mu_B$) is more than that for Cu^{2+} ($1 \mu_B$). Therefore, the increasing Co^{2+} concentration (x) on the octahedral sites may result in an increasing magnetic moment per formula of and $\text{Cu}_{0.61-x}\text{Co}_x\text{Zn}_{0.39}\text{Fe}_2\text{O}_4$ ($0 \leq x \leq 0.5$) an enhancement of magnetization. Magnetization decreases for $x > 0.3$ this may be due to the following fact.

As the percentage of Co^{2+} increases from 0.3 to 1, the M_s value gets decreased. Similarly, an increase of a and or b shift the magnetization value to lower side explains low M_s value for $x \leq 0.3$. The net magnetic moment (n_B Cal.) is given by the sum of the magnetic moments of A and B sublattices, i.e., $M_S = M_B - M_A$. For Co^{2+} substituted Cu-Zn ferrite, Co^{2+} substitution for Cu^{2+} ions at B site, leading to a increase in the B site sublattice magnetization. Moreover, the Fe^{3+} ($5\mu_B$) ions are replaced by less magnetic Cu^{2+} ($1\mu_B$) ions of A-site, leading to a decrease in the A site sublattice magnetization, which leads to a increase in the net magnetization. For example, we use the known magnetic moments for Cu^{2+} ($1\mu_B$), Zn^{2+} ($0\mu_B$), and Fe^{3+} ($5\mu_B$). In this study, the cationic distribution, Zn^{2+} ($0\mu_B$) ions are non-magnetic and do not contribute to the sublattice magnetization.

For $\text{Cu}_{0.61-x}\text{Co}_x\text{Zn}_{0.39}\text{Fe}_2\text{O}_4$, $|M_S| = |M_B| - |M_A| = (0.7 \times 5)\mu_B - (0.7 \times 1 + 1.3 \times 5)\mu_B = 3.7 \mu_B$. The observed magnetic moment (n_B Obs.) per formula unit in Bohr magneton (μ_B) was calculated by using the relation [30].

$$n_B = \frac{\text{Mol wt} \times M_S}{5585}$$

where n_B is the magnetic moment of the samples expressed in Bohr magneton. M_s is the saturation magnetization. The values of (n_B) are shown in Fig. 12 & 13.

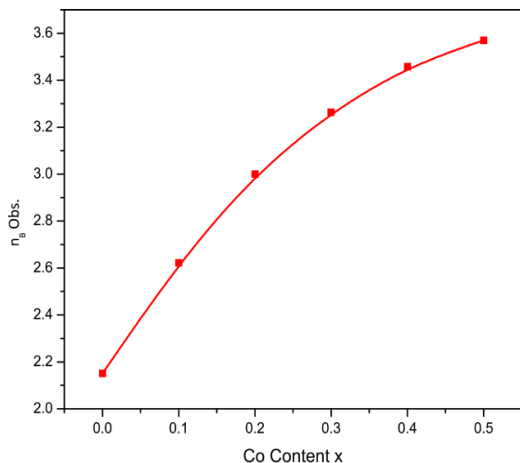


Fig.13 Variation of observed magnetic moment with Co content x .

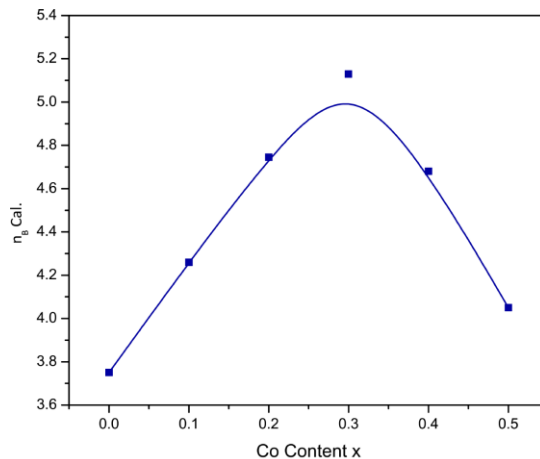


Fig.14 Variation of calculated magnetic moment with Co content x .

Both of them increase up to $x = 0.3$ and then decrease with the increase in Co concentration. Similar reports for saturation magnetization have been quoted by others [31].

$$n_B = (6 + x) \cos \alpha_{Y-K} - 5(1 - x) \quad (5)$$

where x represents Co concentration. The values of Y–K angles are demonstrated in Fig. 10. It increases exponentially with the increase in Co concentration for $x > 0.3$. This shows that in the present system of ferrites, randomness increases as Co is substituted in these Cu ferrites and shows a significant departure from Néel collinear model. The coercive force (H_c) is an independent parameter, which can be altered by magnetocrystalline anisotropy, particle size, porosity, heat deformation and hence is not dependent on saturation magnetization. In this study, the coercive forces tend to rise in increasing Co^{2+} substitution content, in which the values of coercive force varied in the range 100.21- 268.83 Oe (Fig. 15 & 16)

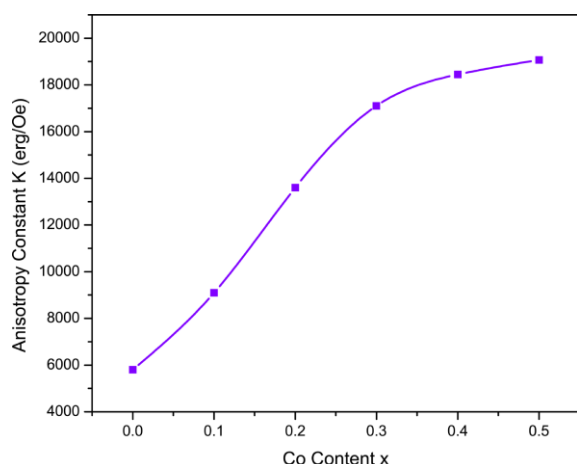


Fig.15 Variation of anisotropy constant 'K' with Co content x.

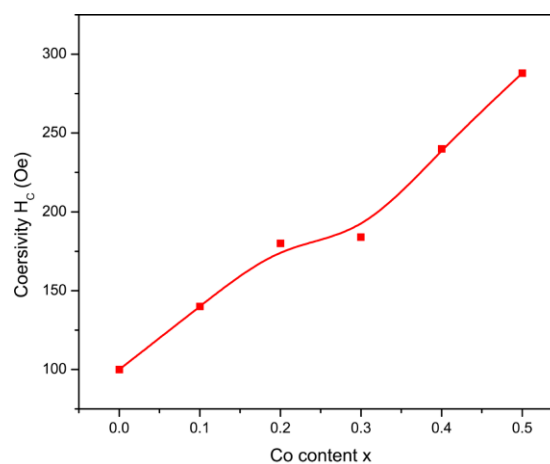


Fig.16 Variation of coercivity 'Hc' with Co content x.

The strong magnetocrystalline anisotropy of the octahedral Co^{2+} ions contributed to the strengthening of the coercive force. There will be a dependence of anisotropy constant K on the Co^{2+} ion concentration x , which can be evaluated by using the relation [37]

$$H_c = \frac{0.98 \times K}{M_s}$$

For all the concentrations Co^{2+} ions system may be considered as isolated Because of the strong dependence of the anisotropy on the location of cations, the measurement of coercivity is a sensitive probe for following cation migrations after increasing Co^{2+} ions. Furthermore, the distortion of the unit cell, the directional order of the octahedral Co^{2+} ions, and the shape anisotropy of the particles combine to render $\text{Cu}_{0.61-x}\text{Co}_x\text{Zn}_{0.39}\text{Fe}_2\text{O}_4$ ferrite powders to become hard magnetic materials with increasing coercivities [38]. The remanent magnetization (M_r) is also an independent parameter since it is not wholly dependent on saturation magnetization (M_s) and coercive force (H_c). The values of remanent magnetization increases from 8.11 to 19.67 emu/gm. Our samples have significance in magnetic recording media, because recording media requires a high saturation magnetization and a moderately high coercivity [39].

IV. Conclusions:

The main conclusions that are derived from the obtained results are:

- Copper nitrate, Cobalt nitrate, zinc nitrate and interacted with ferric nitrate at temperatures starting from 600°C yielding $\text{Cu}_{0.61-x}\text{Co}_x\text{Zn}_{0.39}\text{Fe}_2\text{O}_4$.
- The particle size estimated showed a decreasing trend with the increase in the Co concentration though the preparation condition was identical for all the samples.
- The cation distribution suggests that Co^{2+} and Cu^{2+} both have strong preference towards octahedral B-site, Zn^{2+} also occupy B site by very small amount, whereas Fe^{3+} occupy both A and B site.
- Magnetic measurements shows an increase in M_s value for $x \leq 0.3$ and for $x > 0.3$ shows decreasing trend which suggests, redistribution of cations is occurred at higher Co^{2+} substitution, which ultimately result preferential filling of Co and/or Cu ions in the tetrahedral site.
- Samples have significance in magnetic recording media.

References:

- [1] H.H. Hamdeh, J.C. Ho, S.A. Oliver, R.J. Willey, G. Oliver, G. Busca, J. Appl. Phys. 81 (1997) 1851.
- [2] M. Yokoyama, A. Nakamura, T. Sato, K. Haneda, J. Magn. Soc. Jpn. 22 (Suppl. S1) (1998) 243.
- [3] G. Nicoara, D. Fratiloiu, M. Nogues, J.L. Dormann, F. Vasiliu, Mater. Sci. Forum 235–238 (1997) 145.
- [5] R. Kulkarni, V.U. Patil, J. Mater. Sci. 17 (1982) 843.
- [6] N.S. Satyamurthy et.al Phys. Rev. 181 (2) (1969) 969.
- [7] Muhammad Ajmal, Asghari Maqsood, J. Alloys Compd. 460 (2008) 54
- [10] B.G. Toksha, Sagar E. Shirsath, S.M. Patange, K.M. Jadhav, Solid State Commun. 147(2008) 479.
- [11] Selvan RK, Augustin CO, Berchmans LJ, Saraswathi R. Mater Res Bull 2003;38:41.
- [12] C. G. Whinfrey, D. W. Eckort, A. Tayber, J. Am. Chem. Soc. 82 (1960) 2695
- [13] N. Izaoumen, M. Cherrab, K. Rissouli, K. Benkhouja, K. Jaafari and M. Fahad, J. Phys. IV France 123 (2005) 291
- [14] R.C. Kambale, P.A. Shaikh, S.S. Kamble, Y.D. Kolekar, Journal of Alloys and Compounds 478 (2009) 599
- [15] V. G. Patil, Sagar E. Shirsath, S. D. More, S. J. Shukla, K. M. Jadhav, J. Alloys. Compd. (2009) In press.
- [16] Ovidiu Caltun, G.S.N. Rao, K.H. Rao, B.P. Rao, Ioan Dumitru, Choung-Oh Kim, CheolGi Kim, J. Magn. Magn. Mater. 316 (2007) e618–e620.
- [17] S. M. Patange, Sagar E. Shirsath, B. G. Toksha, S. S. Jadhav, S. J. Shukla, K. M. Jadhav, **Appl. Phys. A: 95 (2009) 429.**
- [18] L. Weil, E. F. Bertaut, L. Bochirou. J. Phys. Radium, 11 (1950) 208.
- [19] B.D. Cullity, Introduction to Magnetic Materials, Addison-Wesley, MA, 1972, p. 141.
- [20] J.B. Goodenough, A.L. Loeb, Phys. Rev. 98 (1955) 391.
- [21] H.N. Ok, Y.K. Kim, Phys. Rev. B 36 (1987) 5120.
- [22] J. Janicki, J. Pietrzak, A. Poresbska, J. Suwalski, Phys. Stat. Sol. (a) 72 (1982) 92.
- [23] H.L. Schl.affer, G. Gliemann, Einf.ührung in die Ligandenfeldtheorie, Akademische Verlagsgesellschaft, Frankfurtam Main, 1967.
- [24] M.D. Sturge, in: F. Seitz, D. Turnbull, H. Ehrenreich (Eds.), Solid State Physics, Vol. 20, Academic Press, New York, 1967.
- [25] J.W. Vrewey, E.L. Heilmann, J. Chem. Phys. 15 (4) (1947) 174–180.
- [26] T. Abbas, Y. Khan, M. Ahmad, S. Anwar, Solid State Comm. 82 (9) (1992) 701–703.
- [27] G. Fagherazzi, F. Garbassi, J. Appl. Crystallogr. 5 (1977) 18.
- [28] C.O. Arean, J.L.R. Blanco, J.M.R. Gonzalez, M.C.T. Fernandez, J. Mater. Sci. Letts. 9 (1990) 229
- [29] C.O. Arean, E.G. Diaz, J.M.R. Gonzalez, M.A.V. Garcia, Solid State Comm. 77 (1988) 275.
- [30] J. Smit, H.P.T. Wijn, Ferrites, Wiley, New York, 1959.
- [31] S.I. Patil and Raka V. Dabhade, IEEE Trans. Mang. 30 (1994) 4915
- [32] L. Néel. C. R. Acad. Sci. Paris 230 (1950) 375.
- [33] O. Caltun, H. Chirac, Lupu., I. Dumitru., P.B. Rao, J. Opto. Adv. Mater. 9 (2007) 1158.
- [34] Y. Yafet, C. Kittel, Phys. Rev. 90 (1952) 295.
- [35] S. S. Bellad, R. B. Pujar, B. K. Chougule, Mater. Chem. Phys. 52 (1998) 166.
- [36] S. S. Jadhav, Sagar E. Shirsath, B. G. Toksha, S. J. Shukla, K. M. Jadhav, Chin. J. Chem. Phys. 21, 381 (2008).
- [37] H. Yangy, Z.Wangy, L. Songy, J. Phys. D: Appl. Phys. 29 (1996) 2574.
- [38] Ph. Tailhades, C. Villette, and A. Rousset, G. U. Kulkarni, K. R. Kannan, and C. N. R. Rao, M. Lenglet, J. Sol. State. Chem. 141, (1998) 56
- [39] Y.L. Li, G.D. Li, Physics of Ferrite, Publishing House of Electronics Industry of Science, Beijing, 1978, p. 514